Anomalous luminescence dynamics of Eu^{3+} in BaFCl microcrystals

X. Y. Chen,[1] W. Zhao,[2] R. E. Cook,[3] and G. K. Liu[1,*]
[1]*Chemistry Division, Argonne National Laboratory, Argonne, Illinois 60439, USA*
[2]*Department of Chemistry, University of Arkansas, Little Rock, Arkansas 72204, USA*
[3]*Materials Science Division, Argonne National Laboratory, Argonne, Illinois 60439, USA*
(Received 9 June 2004; published 17 November 2004)

Spectroscopic properties of Eu^{3+} ions (<0.1 at %) at two main sites of BaFCl microcrystals are investigated. For Eu^{3+} ions at site I the energy levels and luminescence intensity distribution are similar to most other normal systems ever reported. But the $^5D_0$ lifetime of Eu^{3+} at site I decreases rapidly with the temperature and the nonradiative energy transfer (ET) rate is observed to be T^2 dependence. In contrast, Eu^{3+} at site II shows unusual energy level structure and luminescence intensity distribution with the strongest $^5D_0 \rightarrow {}^7F_0$ transition. The nonradiative ET rate of Eu^{3+} at site II obeys a T^9 dependence. Spectroscopic results and theoretical analyses indicate that site II is associated with the charge compensator O^{2-} occupying the nearest F^- site around Eu^{3+}. The mechanisms for anomalous luminescence properties at both sites are further discussed based on the model of charge transfer vibronic exciton (CTVE) and charge-imbalance induced large linear crystal-field potential.

DOI: 10.1103/PhysRevB.70.205122 PACS number(s): 78.55.Hx, 71.70.Ch, 71.23.An, 32.70.Cs

I. INTRODUCTION

Eu^{3+} ions are usually employed as an optical probe to investigate the coordination and environment around the cations substituted in the crystalline lattice based on the fact that the $^5D_0$ (or $^7F_0$) level is nondegenerate and the splitting of the emission (or absorption) transitions reflects the crystal-field (CF) splitting of the nominal ^7F_J (or $^{2S+1}L_J$) levels that depend on site symmetry. The characteristics of the $4f^6$ energy level structure and luminescence line intensity of Eu^{3+} have been extensively investigated in various hosts for several decades. A majority of experimental results can be well interpreted using a standard model of free ion (FI) plus CF interactions established through systematic analyses of the electronic properties of f-element ions in the lanthanide series.[1–3] Due to the large energy gap between the $^5D_0$ and $^7F_6$ ($\sim$12 000 cm^{-1}), the $^5D_0$ lifetime of Eu^{3+} in inorganic solids, usually on the order of millisecond, varies little with the temperature from 2 K to 300 K. Specifically, based on Judd-Ofelt theory,[4] the electronic transitions from the Eu^{3+} $^5D_0$ state to low-lying levels with $J=0$, 3, or 5 are both electric-dipole (ED) and magnetic-dipole (MD) forbidden. The observed weak transitions from $^5D_0$ to these levels are due to CF induced J-mixing effect. However, a series of observations of strong $^5D_0 \rightarrow {}^7F_0$ lines of Sm^{2+} (Refs. 5–8) or Eu^{3+} (Refs. 9–18) ions occupying some particular symmetry sites (C_s, C_n, C_{nv}, $n=1,2,3,4,6$) of crystalline or glass which allows a linear CF parameter have been reported since the 1960s. The role of CF J-mixing has been often overestimated for strong $^5D_0 \rightarrow {}^7F_0$ line in some cases reported.[19] Due to the fact that J-mixing appeared inadequate to explain the magnitude of the intensity or the "hypersensitivity" to local environment, Wybourne[20] and Downer *et al.*[21,22] proposed a mechanism of spin-orbit coupling in the excited configuration (such as $4f^5 5d$) that includes contributions from the third order ED previously neglected in calculating the line-to-line transition intensity. The Wybourne-Downer mechanism is extension of the Judd-Ofelt theory. According to the Wybourne-Downer mechanism, the presence of even a small linear CF term in the CF Hamiltonian could induce a large enhancement to the strength of the $^5D_0 \rightarrow {}^7F_0$ transition given that the energy gap between the intermediate states of opposite parity ($5d$ or charge-transfer states) and the $4f$ states is relatively small. The Wybourne-Downer mechanism thus successfully explained the exceptionally strong $^5D_0 \rightarrow {}^7F_0$ transition of Eu^{3+} in those reported cases.[9,10]

On the other hand, ionic-covalent solids with strong vibronic interaction enable some specific excitations connected with self-consistent charge transfer (CT) and lattice distortion. Charge transfer vibronic exciton (CTVE) in the charge-unbalanced system such as Eu^{3+}:BaFCl crystals can be considered as a bipolaron comprising spatially correlated electron and hole polarons. The theoretical framework of CTVE in solids was first established by Agranovich[23] and Reineker[24] based on a linear exciton-phonon interaction which is induced by modulation of the Coulomb electron-hole attraction, and later developed by Vikhnin.[25–27] The driving force for CTVE formation is charge-transfer-lattice distortion. The leading contribution to such an exciton total energy is indirect electron-hole interaction via lattice with the appearance of the "Negative-U" effect. Strong vibronic energy lowering due to an accompanied lattice relaxation leads to well-defined conditions of CTVE self-trapping.[25,26] Because of charge imbalance and the presence of point defects, multiple sites are expected for trivalent Eu^{3+} ions in BaFCl microcrystals. Previous studies on Eu^{3+} doped bulk BaFCl crystal have observed the existence of more than 15 sites as well as the laser-excitation-induced Eu^{3+} site-to-site conversion for persistent spectral hole burning.[28,29] Based on the model of CTVE in the charge-unbalanced solids, Vikhnin *et al.* have explained the mechanism for multisite structure conversion.[25,26] That is, CTVE-clusters trapped by charged impurities (Eu^{3+} in Ba^{2+} site of BaFCl) are connected with different sites detected in the spectroscopic experiments.

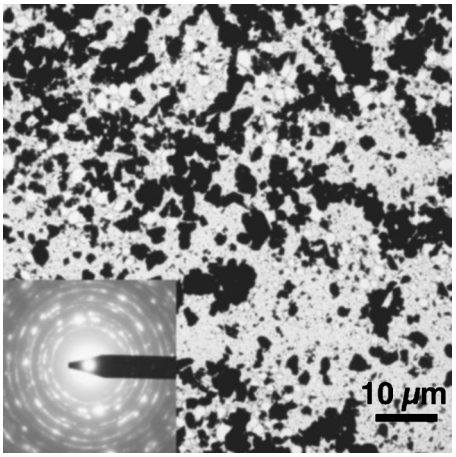

FIG. 1. TEM image of Eu^{3+}:BaFCl microcrystals. The inset shows the electron diffraction patterns of this sample.

This paper reports the experimental evidence of anomalous luminescent dynamics of Eu^{3+}:BaFCl. Interpretation of the experimental results is provided based on the Wybourne-Downer mechanism due to a large linear CF strength in the Eu^{3+}-doped charge-unbalanced systems and the model of CTVE-cluster trapped by charged impurities.

II. EXPERIMENTAL DETAILS

The microcrystals of 0.1 at % Eu:BaFCl were grown by solid-state reaction in the atmosphere of helium. A stoichiometric mixture of BaF_2, $BaCl_2$, and EuF_3 were ground, placed in an Al_2O_3 crucible then heated at 300 °C (1 h) to drive out the moisture and then at 800 °C for one more hour. The top of the sample was covered by active carbon powders. Major Eu^{3+} accompanying with minor Eu^{2+} were contained in the microcrystals. Figure 1 shows the TEM image of the as-prepared particles, with an average particle size of approximately 1–2 μm. The electron diffraction pattern as shown in the inset of Fig. 1 indicates the crystalline phase. Energy dispersive x-ray spectrum (EDXS) confirms that the particles contains Ba, F, and Cl elements. Due to the extremely low doping concentration, the element of Eu was not detected by EDXS. Figure 2 shows the powder x-ray diffraction (XRD) pattern of Eu^{3+}:BaFCl microcrystalline. The line positions match the published diffraction pattern for tetragonal BaFCl (JCPDS #76-1368), which is consistent with the observation by TEM.

For the site-selective luminescence spectra, a pulsed dye laser with a tunable range from 510 to 580 nm, or an ultraviolet (UV) pulsed laser at 266 or 355 nm, was used to pump the samples. The dye laser wavelength was tuned to match the excitation transition $^7F_0 \rightarrow {}^5D_1$ of the Eu^{3+} ions at sites I and II, respectively. The luminescence was dispersed by a monochrometer (SPEX 1704) at a spectral resolution of approximately 0.008 nm and detected with a cooled RCA C31034 photomultiplier. The signals were recorded using a gated boxcar (Stanford Research Systems, model SR250). The sample was mounted in a cryostat with temperature variable from 2 K to 300 K. The luminescence decay measurements were performed using a digital storage oscilloscope (Tektronix TDS 680C).

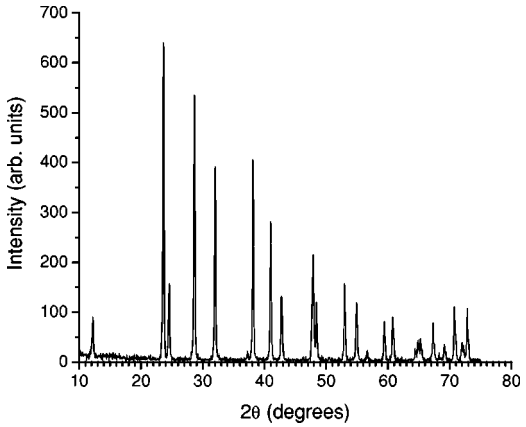

FIG. 2. XRD spectra of Eu^{3+}:BaFCl microcrystals.

III. RESULTS

A. Crystal-field spectra and intensity

When pumped by a laser in the UV region, multiple sites of Eu^{3+} in BaFCl were verified. The main site of Eu^{3+} was determined to be site I for 266 nm laser pumping, and site II for 355 nm laser pumping. At 3 K, sites I and II can be selectively excited to $^5D_1$ by 526.85 nm and 553.62 nm lasers, respectively. The luminescence spectra of sites I and II in the range of 570–640 nm are compared in Fig. 3. The energy levels and relative luminescence intensity from $^5D_0$ to each CF level are summarized in Table I. As shown in Fig. 3 and Table I, the luminescence intensity distribution, CF level splitting of Eu^{3+} at site I are as normal, similar to most other Eu^{3+} systems reported hitherto, with the strongest $^5D_0 \rightarrow {}^7F_2$ and very weak $^5D_0 \rightarrow {}^7F_0$ transitions. Thus we assume

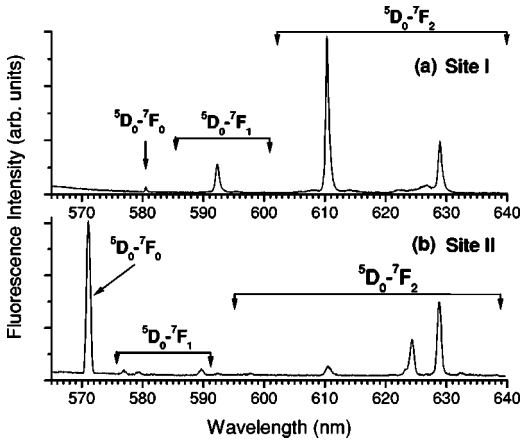

FIG. 3. Luminescence spectra of Eu^{3+}:BaFCl microcrystals at (a) site I, λ_{exc}=526.85 nm and (b) site II, λ_{exc}=553.62 nm. Both spectra were measured at 3.2 K. The luminescence was detected using a boxcar integrator that averaged the luminescence signal from a cooled PMT with 15 μs gate. The delays from the pump laser pulse were set at 0.10 ms and 0.23 ms for (a) and (b), respectively.

TABLE I. Energy levels and relative luminescence intensities from $^5D_0$ of Eu^{3+} at two main sites in BaFCl microcrystals at 3 K.

	Site I		Site II	
Multiplet	Energy (cm^{-1})	Intensity	Energy (cm^{-1})	Intensity
$^7F_0$	0	3.1	0	100
$^7F_1$	293	0.5	176	2.9
	343	18	249	2.5
	432	1.2	549	5.3
$^7F_2$	781	2.0	780	2.3
	842	100	1145	1.4
	942	2.0	1494	25
	1271	5.0	1607	47
	1326	32	1699	2.5
$^7F_3$	1865	0.9	1929	0.3
	1948	1.1	1966	0.2
	1970	6.4	2154	0.4
			2237	1.7
			2330	0.2
			2348	0.15
			2411	0.2
$^4F_4$	2466	0.5	3018	1.8
	2811	0.1	3064	0.2
	2834	0.2	3099	0.4
	2871	1.2	3150	3.5
	2975	0.2	3164	3.0
	3013	0.3	3206	0.4
	3080	3.3	3270	0.9
	3089	5.9	3283	1.5
	3121	2.9	3292	1.3
$^7F_5$	3782	1.2	3700	0.04
	3977	0.06	3843	0.08
	4000	0.09	3954	0.05
	4194	0.04	4063	0.16
			4426	0.13
$^7F_6$	Not observed		4694	1.7
			4806	0.03
			4874	0.05
			4952	0.09
			4979	0.08
			5049	0.02
			5247	0.04
$^5D_0$	17227		17512	
$^5D_1$	18981		18063	

that Eu^{3+} at site I substitute the Ba^{2+} site with an approximate C_{4v} symmetry in the lattice, the CF environment of which is weakly distorted by the CTVE effect due to the charge imbalance around Eu^{3+}.

As for Eu^{3+} ions at site II, the luminescence intensity distribution appears anomalous with the strongest $^5D_0 \rightarrow {}^7F_0$ and second strongest $^5D_0 \rightarrow {}^7F_2$ transitions (Fig. 3 and Table I). This anomalous result cannot simply be ascribed to

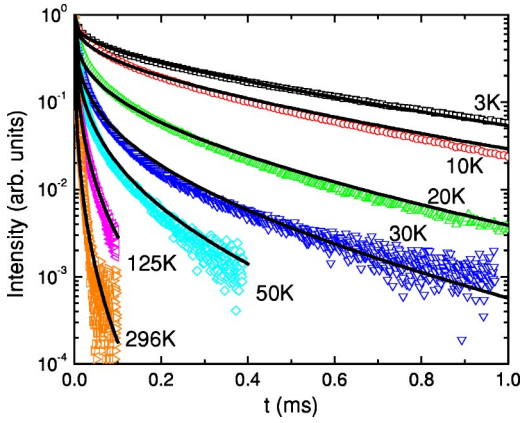

FIG. 4. (Color online) Luminescence decay from the $^5D_0$ of Eu^{3+} ions at sites I in Eu^{3+}:BaFCl microcrystals at various temperatures (3–296 K). The scattering points are experimental, and the solid curves are the fitting results.

J-mixing effect. Compared to the range 18900–19100 cm^{-1} found in most crystals, the $^5D_1$ level of Eu^{3+} at site II is located at an unusually low position (18063 cm^{-1}), which leads to the most narrow gap (only 551 cm^{-1}) between $^5D_1$ and $^5D_0$ among those ever reported (usually about 1700 cm^{-1}). The unusually high position of the $^5D_0$ level (17512 cm^{-1}) exceeds most of the values reported for other Eu^{3+}-doped crystalline compounds. The CF level splitting of $^7F_2$ is observed to be as wide as 919 cm^{-1}. Similar CF spectra were also found in some charge-unbalanced hosts such as oxyapatite or strontium fluorapatite.[13,18] The characteristics of standard and anomalous CF spectra of Eu^{3+} in some inorganic crystal hosts has recently been reviewed in Ref. 30.

B. Temperature dependence of luminescence lifetimes

In order to investigate the luminescence dynamics of Eu^{3+} ions at sites I and II, the luminescence decay of the $^5D_0$ state in Eu^{3+}:BaFCl microcrystals at different temperatures was measured. The observed decay curves for sites I and II at various temperatures are compared in Figs. 4 and 5, respectively. The decay curves of site I at all temperatures are significantly nonexponential, whereas the decays from Eu^{3+} at site II are single exponential from 3 K up to 180 K. Although the doping concentration of Eu^{3+} is less than 0.1 at %, the luminescence of site II is significantly quenched at higher temperatures. This makes the lifetime measurement of site II difficult at temperature above 180 K because the weak luminescence of Eu^{3+} at site II is mixed with the broadened emission lines of other defect sites which have less temperature dependence. Both decays of sites I and II are sensitive to temperature with no rising time, contrary to the normal Eu^{3+} decay characteristics of $^5D_0$.

C. Relevant experimental evidence of anomalous Eu^{3+} dynamics

The following evidence further supports the existence of the anomalous site II in Eu^{3+}:BaFCl. First, to study the persistent spectral hole burning in the bulk Eu^{3+}:BaFCl

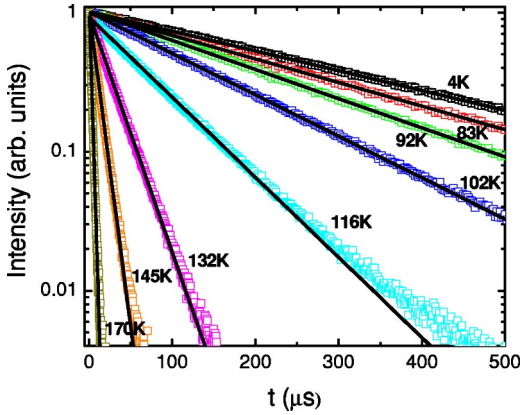

FIG. 5. (Color online) Luminescence decay from the $^5D_0$ of Eu^{3+} ions at sites II in Eu^{3+}:BaFCl microcrystals at various temperatures. The scattering points are experimental, and the solid curves are the fitting results.

(0.1 at %) crystals which were grown in air by the Bridgman method, Liu *et al.*[28,29] previously observed that many other sites, instead of site II, dominate the emission spectra while the bulk Eu^{3+}:BaFCl crystals were pumped by a 355 nm laser, as shown in Fig. 6(a). When pumped by a single-frequency laser at 571.08 nm which corresponds to the $^7F_0 \rightarrow {}^5D_0$ transition, the site-selective luminescence lines were coincident with those shown in Fig. 3(b), which indicates that site II lines were also formed but not dominant in those bulk crystals. In contrast, the site II lines almost disappear in the same bulk Eu^{3+}:BaFCl crystals which were grown in the atmosphere of argon to reduce the oxygen defect according to the site-selective laser spectroscopy.[31] Secondly, after 5

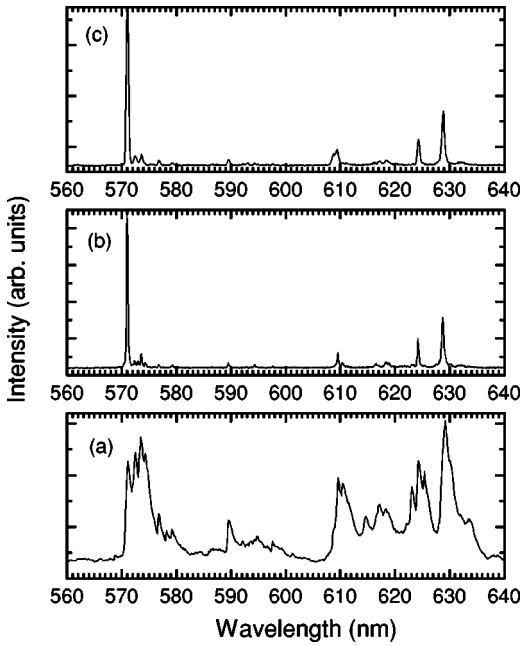

FIG. 6. Comparison of the luminescence spectra of Eu^{3+} ions in (a) BaFCl bulk crystals; (b) BaFCl bulk crystals aged for 5 years; and (c) BaFCl microcrystals. The spectra were measured at 77 K when pumped by a pulsed 355 nm laser.

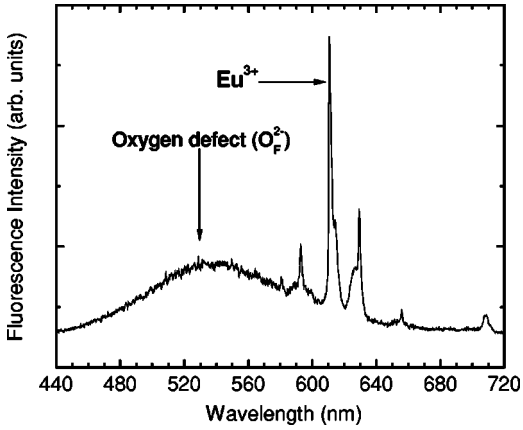

FIG. 7. Luminescence spectra of Eu^{3+}:BaFCl microcrystals at 30 K when pumped by a 266 nm laser, showing the emission band of oxygen defect ($O_F{}^{2-}$). The emission was detected with 15 μs gate, and the delays from the pump laser pulse were set at 0.10 ms.

-year-aging in air, site II became dominant in the crystals grown in air with thickness less than 1 mm. The luminescence spectrum of the aged crystals is very similar to that of the microcrystal counterparts, as compared in Figs. 6(b) and 6(c). The lifetime of Eu^{3+} ions at site II is distinct, and has the same temperature-dependence either in the aged bulk crystals or the microcrystals. The above facts indicate that oxygen defects in BaFCl lattice may participate in the structure formation of site II. Although the microcrystals were initially synthesized in the atmosphere of helium, the smaller particle size and active surface may facilitate oxygen adsorption and penetration and the formation of oxygen defect during the post-synthesis treatment in the air. Thirdly, the possibilities of assigning the observed lines to other divalent or trivalent rare-earth (RE) impurities such as Pr^{3+}, Sm^{2+}, Sm^{3+}, and Dy^{3+} can be clearly ruled out because of differences in energy and the distinct behavior of temperature-dependent lifetimes.

In particular, we have also observed the luminescence of oxygen defects in addition to the emission from site I when the sample was excited by a 266 nm laser. As shown in Fig. 7, the broadband luminescence in the visible (peaking at ~540 nm, with a lifetime of 0.35 ms at 2.5 K) originates from the oxygen defects ($O_F{}^{2-}$, or O^{2-} substituting one of the nearest F^- site around Eu^{3+}), which is usually termed as type I oxygen defects in BaFCl crystals.[32]

IV. DISCUSSION

A. Possible mechanisms for the observed T^n dependence

To date, there are few reports on the temperature-dependence of energy transfer from the $^5D_0$ state of Eu^{3+} doped in inorganic crystals. Bettinelli *et al.* reported the markedly nonexponential decay of luminescence from the $^5D_0$ at 12 K in stoichometric $Cs_2NaEuCl_6$ crystals.[33] They ascribed the complex kinetics to energy migration and energy transfer to defects and relaxation at both defect and regular sites at competitive rates. Similar decay behaviors of $^5D_0$ and ET mechanisms were also reported and discussed in

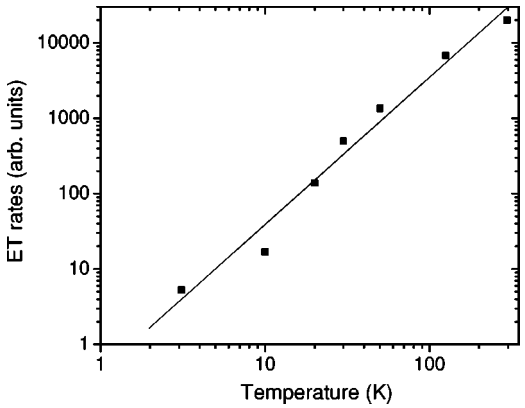

FIG. 8. Nonradiative ET rate of Eu^{3+} ions at site I as a function of temperature. The scattering points are experimental, and the lines are the fitting results.

$EuAl_3B_4O_{12}$ (Ref. 34), $EuMgB_5O_{10}$ (Ref. 35), $Eu_2(MoO_4)_3$ (Ref. 36), and Eu_2O_3 (Ref. 37) previously. As for Eu^{3+} diluted in crystals, Buijs *et al.* reported the temperature dependence of Eu^{3+} site-to-site ET rates in Gd_2O_3 (Ref. 37) and β'-$Gd_2(MoO_4)_3$ (Ref. 36) crystals. In the Eu^{3+}(0.1 at %):BaFCl crystals we studied, the decays of $^5D_0$ luminescence of Eu^{3+} at site I can be well fitted by the Inokuti-Hirayama model.[38–40] The decay of the site I luminescence obeys,

$$\ln I(t) - \ln I(0) = -t/\tau_0 - \frac{4}{3}\pi c_a r_0^3 [W_0(T)t]^{3/s}\Gamma\left(1-\frac{3}{s}\right), \tag{1}$$

where c_a is the concentration of acceptor trapping the Eu^{3+} at site I and r_0 is the nearest neighbor distance corresponding to the donor-acceptor transfer rate W_0. $\Gamma(1-3/s)$ is the Gamma function, and $s=10$ stands for quadrupole-quadrupole interaction. The radiative lifetime of Eu^{3+} at site I, τ_0, was measured to be 0.779 ± 0.001 ms. The fitted decay curves of sites I from 3 K to 296 K are shown in Fig. 4. The very good agreement between the observed and fitted decay curves at all temperatures indicates the success of Inokuti-Hirayama model for site I. The temperature-dependent ET rates, $W_0(T)$, can be extracted by fitting the decays of site I from 3 K to 296 K with Eq. (1), as shown in Fig. 8. Figure 8 clearly shows that W_0 is proportional to $T^n(n=2.0\pm0.1)$.

The ET rates of Eu^{3+} at both sites are very sensitive to temperature, thus suggest that phonon-assisted ET processes are dominant nonradiative relaxation mechanism. The theory of diagonal phonon-assisted ET processes has been systematically formulated by Holstein *et al.*[41] In Table II, the approximate temperature-dependent ET rate are summarized according to different microscopic mechanisms. The limitations to derive these results were addressed in details in Ref. 41. In general, a T^3 dependence of phonon-assisted ET rate can be ascribed to two-phonon two-site nonresonant process, while a T^1 dependence is due to direct one phonon process. Therefore we conclude that the ET mechanisms of Eu^{3+} at site I might involve both two-site nonresonant and direct one phonon processes which on the average leads to the observed T^2 dependence. The nonexponential decay of site I also provides a direct experimental evidence of the existence of CTVE-connected cross-relaxation for site conversion assumed by Vikhnin *et al.*[25,26] Similarly, Buijs *et al.* had observed one-phonon assisted ET at very low temperatures and two-phonon two-site nonresonant ET at higher temperatures from the $^5D_0$ of Eu^{3+} ions in β'-$Gd_2(MoO_4)_3$ crystals.[36]

TABLE II. Approximate temperature-dependent phonon-assisted ET mechanism.[a]

Mechanism	T-dependency
Direct one phonon	$W_{ij}\propto T$
Two phonon: 2-site nonresonant	$W_{ij}\propto T^3$
Two phonon: 1-site Raman	$W_{ij}\propto T^7$(Short λ_{phonon})
	$W_{ij}\propto T^9$(Long λ_{phonon})
Two phonon: 1-site resonant	$W_{ij}\propto \exp(-\Delta/kT)$
Two phonon: 1-site nonresonant	$W_{ij}\propto T^7$

[a]From Ref. 41. W_{ij} is the ET rate from ion site i to site j; Δ is the splitting to real state; λ_{phonon} is the wavelength of the involved phonons to make up the energy mismatch between site i and j.

The temperature-dependent lifetime of Eu^{3+} at site II behaves very differently from that of site I. The exponential decay shows no rising time within the detectable limit, in accordance with the observed small energy gap between $^5D_1$ and $^5D_0$. The measured lifetime at 3 K (305.3 μs) is reasonably assumed to be the radiative lifetime (τ_0) of Eu^{3+} at site II since the lifetime observed varies little below 34 K. Assuming the radiative lifetime of site II is independent of the temperature, the temperature-dependence of phonon-assistant ET rates of Eu^{3+} at site II is calculated based on the observed lifetime ($\tau(T)$) according to $W_{NR}(T)=\tau(T)^{-1}-\tau_0^{-1}$ and shown in Fig. 9. Figure 9 shows a T^n ($n=9.1\pm0.1$) dependence for W_{NR} with temperature. Note that the deviation from the fitted line at 34 K in Fig. 9 is possibly due to the uncertainty of lifetime measurement since a tiny fluctuation of the observed lifetime may mask the extremely low nonradiative ET rates. As a matter of fact, the fitted lifetimes from

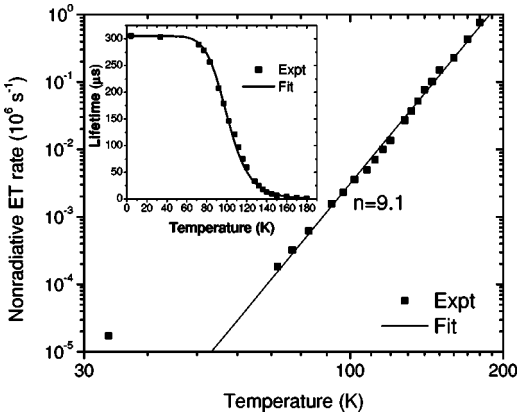

FIG. 9. Nonradiative ET rate of Eu^{3+} ions at site II as a function of temperature. Inset shows the temperature-dependent lifetime. The scattering points are experimental, and the lines are the fitting results.

3 K to 180 K are in good agreement with the experimental values, as shown in the inset of Fig. 9. Assuming the validity of the T^9 dependence at room temperature, the lifetime at 300 K is extrapolated to be approximately 14 ns, shortened by more than 4 orders of magnitude in comparison with the lifetime at 3 K.

The unusual T^9 dependence of nonradiative relaxation rates for Eu^{3+} at site II as shown in Fig. 9, cannot be ascribed to a process of direct multi-phonon relaxation, since the maximum phonon frequency of BaFCl microcrystal was observed to be 294 cm^{-1} and thus at least 40 phonons are needed to bridge the energy gap between $^5D_0$ and $^7F_6$ ($\sim$12 000 cm^{-1}). The contribution from the local vibrational modes of impurities induced by O^{2-} defect can also be ruled out for the same reason, since the maximum localized vibrational frequency of the axial Eu^{3+}-O^{2-} cluster at site II is reasonably assumed to be less than 600 cm^{-1} based on the reported values for other similar systems.[13,42] Among those possible phonon-assisted ET processes (Table II), direct one phonon and two-site nonresonant processes that have weak power dependence of temperature can also be ruled out. One-site resonant or nonresonant processes are not applicable to the $^5D_0$ state, because they both require the existence of the third electronic level nearby.[41] Finally, within the currently available theoretical framework, we infer the two-phonon one-site Raman ET process as the primary mechanism for the observed excited state dynamics of Eu^{3+} at site II. As predicted by Holstein,[41] one obtains a temperature dependence proportional to T^9 for one-site Raman ET rate at the temperature much lower than the Debye temperature ($\sim$468 K),[43] by taking into account the significant contribution of coherence factor and assuming long phonon wavelength in his formula. For the short phonon wavelength approximation, a T^7 dependence is theoretically predicted. Nevertheless, so far we have no evidence to exclude the contributions from other ET mechanisms than two-phonon one-site Raman ET processes for the temporal behaviors of site II. On the other hand, the observed single-exponential decay of site II at different temperatures may also indicate ultra-rapid donor-donor transfer (supermigration or superexchange), followed by a quenching to traps at a comparatively slow rate, according to Huber's theory.[40] The nature of this ultra-rapid donor-donor transfer in the microcrystals is expected to be related to the exciton hopping trapped by Eu^{3+} at site II, which deserves further studies.

B. CTVE model of sites I and II

To understand the CTVE effect on the anomalous luminescence dynamics, we propose the structural CTVE models for Eu^{3+} at sites I and II based on the spectroscopic results. The assumed structures of the nearest neighbor ligands around the Eu^{3+} ion at sites I and II are shown in Figs. 10(a) and 10(b), respectively. Due to CTVE, the symmetry of site I is slightly distorted from C_{4v} toward C_{2v}. Recently, a standard CF levels fitting has been performed according to C_{2v} site symmetry for site I with a moderate rms deviation ($\sim$23 cm^{-1}).[30] Our spectroscopic results show that the CF environment of Eu^{3+} at site II is strongly distorted by the

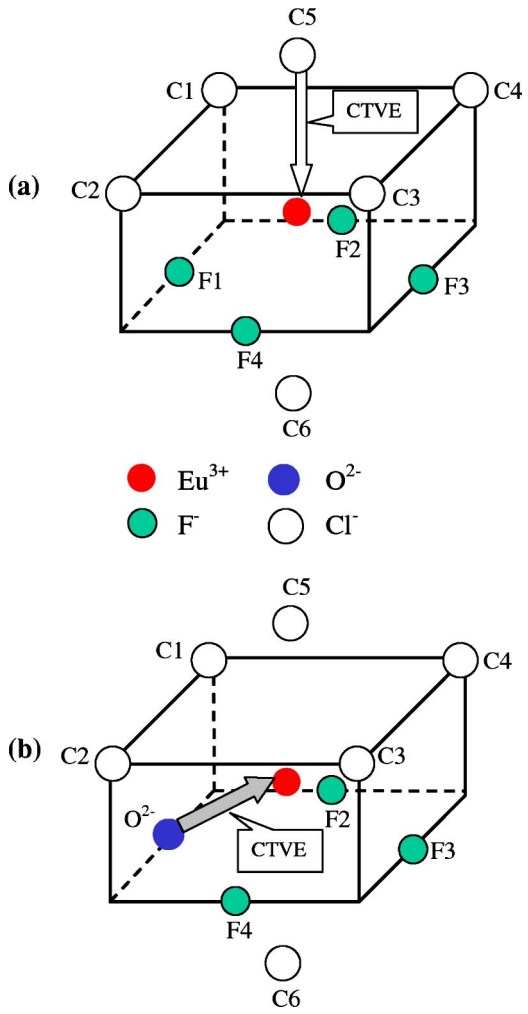

FIG. 10. (Color online) Proposed structures of the nearest neighbor ligands around the Eu^{3+} ion at (a) site I; (b) site II in BaFCl microcrystals. In (a), only the $Cl^- \rightarrow Eu^{3+}$ charge transfer channel (from the nearest Cl^-) induced by Eu^{3+} charged impurity is taken into account. For simplicity, charge transfers from other neighboring Cl^- ions (C1, C2, C3, C4, and C6) are ignored. In (b), the oxygen defects act as the charge compensator of Eu^{3+} by substituting the nearest F^- with strong CTVE effect.

CTVE effect. As mentioned in Sec. III C, the oxygen defects may play an important role for the structure of site II. In Fig. 10(b), the unavoidable oxygen defects act as the charge compensator of Eu^{3+} by substituting the nearest F^-. The symmetry of site II is C_s. Note that the distances from Eu^{3+} to C5, O^{2-} (or F1, F2, F3, F4), C1 (or C2, C3, C4), and C6 in Fig. 10 are approximately 0.320 nm, 0.265 nm, 0.329 nm, and 0.403 nm, respectively, determined from the crystal structure data.[44,45] Our attempts to perform the CF level fitting of Eu^{3+} at site II by the standard CF model did not result in good agreement between the experimental data and calculations. This also happened in some other Eu-doped charge-unbalanced systems, such as $Sr_5(PO_4)_3F$.[18] This discrepancy may be possibly due to (1) drastic changes in the free ion parameters at site II in views of the large energy level shifts such as that of the $^5D_1$ state; (2) inaccurate energy level assignment because of the appearance of other indistinguish-

able sites or missing lines; or (3) the failure of standard CF modeling, as will discussed in the following section. However, in comparison with the CF splittings at site I, the CF strength of Site II is obviously much larger than that of site I. The existence of large CF strength is typical in some other hosts in which anomalous Eu^{3+} CF spectra were identified.[30]

In comparison with the radiative lifetime (1–20 ms) of the $^5D_0$ of Eu^{3+} in other crystals or site I in BaFCl, the radiative lifetime of site II (~0.3 ms) is significantly reduced, which might suggest the important role of CTVE effect on the $4f$-$4f$ electronic transitions. As observed before, the stronger CF interaction or lower CT sates of Eu^{3+} may lead to the shorter radiative lifetime of $^5D_0$ according to the mechanism of intensity borrowing from CT transitions via the $4f^6$-CT configurational mixing.[46]

C. Linear crystal-field potential and Wybourne-Downer mechanism

In this section, special emphasis will be given to the Wybourne-Downer mechanism which is very important for understanding the anomalous branch ratios of the luminescence spectrum we observed for Eu^{3+} at site II. Obviously, the CTVE at site II is much stronger than that at site I due to the role of oxygen ion. An equilibrium value of the Eu-O distance decreasing in the CTVE at site II is significantly stronger than the Eu-Cl distance decreasing in the CTVE at site I. Simultaneously, the equilibrium CTVE charge transfer for the site II is more significant than for that of site I. These facts jointly lead to a large linear CF potential in site II. The strength of linear CF potential is generally measured by the scalar linear CF rotational invariant defined by $S_1=(\frac{1}{3}\Sigma_{q=0,\pm1}|A_{1q}|^2)^{1/2}$, where A_{1q} is the linear CF component.[6,8,21] S_1 is invariant under arbitrary rotations of the crystal lattice, similar to the common even-order CF strengths S_k $(k=2,4,6)$.[47] Approximately, by taking into account point-charge model and 9 nearest neighboring ligands shown in Fig. 10, the estimated value of S_1 significantly increases from 6 714 $cm^{-1}/Å$ for site I to 14 425 $cm^{-1}/Å$ for site II, which confirms the above hypothesis. It has been reported that in several oxide matrices (such as Sr_2TiO_4, $Ca_5(PO_4)_3F$ and $Sr_5(PO_4)_3F$) Eu^{3+} ion substitutes a divalent cation and exhibits unusually strong $^5D_0\rightarrow{}^7F_0$ line intensity due to the charge-imbalance induced large linear CF potential.[9,13,17,18,48] The CT states of such Eu^{3+} doped materials are known to be fairly low in energy compared with those in other oxide hosts.[48] Similarly, for Eu^{3+} at site II in BaFCl, the Eu-O CT states as well as Eu-Cl (or Eu-F) CT states locate at much lower levels than those of Eu^{3+} $4f^55d$ states, which thus act as intermediate states to induce the forced second order and third order ED transition. This has been confirmed by the observation of Su *et al.* that the Eu-Cl CT states ($4f^73p^{-1}$) in Eu^{3+}:BaFCl crystals lie approximately at 41 500 cm^{-1}.[49] It is expected that the Eu^{3+}-O^{2-} CT energy is even lower than that of the Eu^{3+}-Cl^- in views of the structural stabilization from oxygen impurity charge compensation at site II. Chen *et al.* reported that the lowest Eu^{3+}-O^{2-} CT states in Eu^{3+}:$BaF_{0.95}Cl_{1.05}$ or Eu_2O_3 crystals lie at ~35 000 cm^{-1}.[50] Based on the Wybourne-Downer mechanism (the third order ED intensity), the line strength of the $^5D_0\rightarrow{}^7F_0$ transition which borrows intensities from the CT transitions is proportional to ${S_1}^2/{\Delta_{CT}}^4$ according to a rederivation similar to Judd's and Downer's original papers, where Δ_{CT} is the mean energy difference between $4f^6$ and the intermediate CT configurations.[4,6,8,21] As can be seen from this relationship, the third order ED intensity is inversely proportional to the fourth power of Δ_{CT} thus should be much more sensitive to the location of intermediate CT states than the second order ED intensity ($\propto{\Delta_{CT}}^{-2}$). Therefore, both the relatively low $Eu^{3+}-O^{2-}$ CT states and large linear CF strength for Eu^{3+} at site II may lead to a very strong $^5D_0\rightarrow{}^7F_0$ intensity as we observed. Furthermore, as pointed out by Downer *et al.*[21,22] and Shen *et al.*[8] and Tanaka *et al.*,[6,7] the third order ED interaction, which exclusively contributes to the $^5D_0\rightarrow{}^7F_0$ line intensity, may significantly cancel the second order ED transition of the $^7F_0\rightarrow{}^5D_2$ (or $^5D_0\rightarrow{}^7F_2$) lines due to the opposite sign. It is expected that, by taking into account the CT states as the intermediate states, this cancellation also holds and accounts for the weak $^5D_0\rightarrow{}^7F_2$ luminescence intensity of site II. As a result, the $^5D_0\rightarrow{}^7F_0$ intensity is experimentally observed to be even larger than that of the $^5D_0\rightarrow{}^7F_2$ transitions if such a strong cancellation occurs. So far, a quantitative intensity analysis like those reported in Refs. 8 and 21 is still lacking due to theoretical difficulties in defining the quantum states and covalency of the CT intermediate states. Nevertheless, the Wybourne-Downer mechanism should play a dominant role in the $^5D_0\rightarrow{}^7F_0$ line intensity. The anomalous branch ratios of the luminescence intensity for Eu^{3+} at site II as well as in other hosts[9–18] can be explained based on the Wybourne-Downer mechanism. However, the significant shift of the centroid of multiplets of Eu^{3+} at site II is not well understood within the standard CF model. The observed large line shift from the multiplets of Eu^{3+} free-ion state might indicate the considerable changes in electrostatic and spin-orbit interactions. Such changes are induced possibly by the CTVE-enhanced covalent effect of Eu-O bonding or orbital mixing. As pointed out by Hoshina *et al.*[46] and Jørgensen,[51] the spin-restricted covalency effect may further modify the line positions of ^7F multiplets of the $4f^6$ configuration due to their interaction with the lowest septet CT states of the $4f^7(^8S)$ +hole configuration, while the ^5D_J states are mainly affected by the central field covalency effect. Further studies of relationship between the CF level fitting including both FI and CF parameters and CTVE mechanism (or covalency effect) are required to confirm the above hypothesis. A modified ligand-field theory similar to the treatment in the exchange charge model[52] is needed.

In an effort to interpret the anomalous luminescent properties of site II, we also noticed the quantum-confinement-induced ligand-RE hybridization theory proposed by Bhargava for explaining the lifetime shortening from ms to ns in nanocrystals of Mn^{2+}:ZnS.[53] Apparently, this theory might well interpret what we have observed, since not only the lifetime of Eu^{3+} ions but also the intensity distribution (or oscillator strengths) and line positions are significantly changed for Eu^{3+} at site II, which strongly support the hypothesis of *sp-f* mixing (hybridization) in the RE ions. How-

ever, we gave up this kind of mechanism for the following two reasons: (1) TEM results reveal that the particle size of Eu:BaFCl microcrystals is approximately $1-2\ \mu$m, therefore, the quantum confinement effect is negligible; (2) Bhargava's experimental results have been challenged by several authors[54–56] and the ligand-RE hybridization theory lack of clear experimental evidence. For example, similar to his controversial finding on the nanocrystal of Mn^{2+}:ZnS, Bhargava[57] had ever reported that the lifetime of Tb^{3+} was greatly shortened from ~ 3 ms in the bulk phosphors to 7 ns in 2–5 nm ZnS nanocrystals. Unfortunately in his paper the luminescence intensity distribution and line positions from $^5D_4$ of Tb^{3+} ions was not significantly changed, which makes his assumption less convincing.[58]

Nevertheless, due to the very short $Eu^{3+}-O^{2-}$ distance (0.265 nm) at site II, we have no reason to exclude such a possibility that the two ions' orbital overlap is enhanced by charge compensation thus leads to unusual ligand-RE hybridization.

V. CONCLUSIONS

In summary, we have observed anomalous spectroscopic properties of Eu^{3+} at two crystallographic sites of BaFCl microcrystals. Eu^{3+} ions at site I show normal CF splitting and luminescence intensity distribution except for rapid energy transfer from 3 K up to room temperature. The energy transfer of Eu^{3+} at site I may be induced by both two-site nonresonant and direct one phonon processes which on the average leads to the observed T^2 dependence. Due to the strong distortion of CF environment and a large linear CF potential enhanced by charge-imbalance, Eu^{3+} ions at site II not only exhibit distinct luminescence intensity distribution and lineshifts, but also show unusual temperature-dependent $^5D_0$ lifetime. The unusual T^9 dependence of the nonradiative relaxation rates from the $^5D_0$ state of Eu^{3+} at site II could be possibly ascribed to two-phonon one-site Raman ET processes. The CTVE model for Eu^{3+} at sites I and II is proposed for explaining the spectroscopic experiments. Specifically, the structure of site II is formed due to the ubiquitous oxygen defects which act as the charge compensator of Eu^{3+} by substituting the nearest F^-. The oxygen defect thus induces a strong CTVE effect. The experimental evidence of ET at sites I and II may further confirm previous assumptions that CTVE-connected cross-relaxation is responsible for excitation-induced site conversion. These findings suggest the potential use of Eu^{3+} at site II as an environmental (e.g., temperature and oxygen pressure) sensor as well as a structural probe. It is predicted that anomalous luminescence properties like Eu^{3+} at site II may also be observed in the Eu^{3+}-doped charge-compensated systems in which there exist a large linear CF potential and low-lying CT states. We have also shown that, in particular, the luminescence dynamics of Eu^{3+} at site II in BaFCl microcrystals is strongly affected by the CTVE and the linear CF potential. Given that Eu^{3+}:BaFCl crystals may have potential applications in optical data storage, signal processing and flat panel display devices, fundamental understanding of the CTVE effect and Wybourne-Downer mechanism that are enhanced by charge-imbalance on the rare earth luminescence dynamics is of great importance.

ACKNOWLEDGMENTS

Work at Argonne National Laboratory was performed under the auspices of the Office of Basic Energy Science, Division of Chemical Sciences, U.S. Department of Energy, under Contract No. W-31-109-ENG-38. The authors are grateful to M.F. Reid for the *f*-shell empirical modeling program and to B.Z. Malkin and V.S. Vikhnin for helpful discussion.

*Author to whom correspondence should be addressed. Electronic address: gkliu@anl.gov

[1] C.A. Morrison and R.P. Leavitt, in *Handbook on the Physics and Chemistry of Rare Earths*, edited by K.A. Gschneidner, Jr. and L. Eyring (North-Holland, Amsterdam, 1982), Vol. 5, Chap. 46, p. 584.

[2] W.T. Carnall, G.L. Goodman, K. Rajnak, and R.S. Rana, J. Chem. Phys. **90**, 3443 (1989).

[3] C. Görller-Warland and K. Binnemans, in *Handbook on the Physics and Chemistry of Rare Earths*, edited by K.A. Gschneidner, Jr. and L. Eyring (North-Holland, Amsterdam, 1996), Vol. 23, Chap. 155, p. 121; (North-Holland, Amsterdam, 1998), Vol. 25, Chap. 167, p. 101.

[4] B.R. Judd, Phys. Rev. **127**, 750 (1962); G.S. Ofelt, J. Chem. Phys. **37**, 511 (1962).

[5] Z.J. Kiss and H.A. Weakliem, Phys. Rev. Lett. **15**, 457 (1965).

[6] M. Tanaka and T. Kushida, Phys. Rev. B **53**, 588 (1996).

[7] T. Kushida and M. Tanaka, Phys. Rev. B **65**, 195118 (2002).

[8] Y.R. Shen and K.L. Bray, Phys. Rev. B **58**, 11944 (1998).

[9] W.C. Nieuwpoort and G. Blasse, Solid State Commun. **4**, 227 (1966).

[10] G. Blasse and A. Bril, J. Chem. Phys. **46**, 2579 (1967).

[11] J. Hölsa and P. Porcher, J. Chem. Phys. **75**, 2108 (1981).

[12] J. Hölsa and P. Porcher, J. Chem. Phys. **76**, 2790 (1982).

[13] B. Piriou, D. Fahmi, J. Dexpert-Ghys, A. Taitai, and J.L. Lacout, J. Lumin. **39**, 97 (1987).

[14] J. Hölsa and M. Karppinen, Eur. J. Solid State Inorg. Chem. **28**, 135 (1991).

[15] D. Zakaria, R. Machiou, D. Zambon, and M.T. Fournier, Eur. J. Solid State Inorg. Chem. **28**, 109 (1991).

[16] N.J. Cockroft, S.H. Lee, and J.C. Wright, Phys. Rev. B **44**, 4117 (1991).

[17] A. Zounani, D. Zambon, and J.C. Cousseins, J. Alloys Compd. **207-208**, 94 (1994).

[18] A.O. Wright, M.D. Seltzer, J.B. Gruber, and B.H.T. Chai, J. Appl. Phys. **78**, 2456 (1995).

[19] For instance, the $^5D_0 \rightarrow {}^7F_0$ line was observed to be the strongest among those transitions from the same $^5D_0$ state in Eu^{3+}:LaOBr

(Ref. 12). Unfortunately, the large B_{20} CF parameter ($-1500\ cm^{-1}$) obtained by the CF fitting misled the authors to conclude that *J*-mixing made the major contribution to the appearance of the strong $^5D_0 \rightarrow {}^7F_0$ line. To clarify this, we have performed the CF fitting for Eu^{3+}:LaOBr by the complete diagonalization including both FI and CF parameters without wave functions truncation of the basis set. A careful refitting the CF levels including the excited $^5D_{0\text{-}2}$ states of Eu^{3+}:LaOBr yields the similar CF parameters as those in Ref. 12 but shows only 9% *J*-mixing from $^7F_2$ to $^7F_0$. Obviously, it is impossible for such a low extent of *J*-mixing to induce the strongest $^5D_0 \rightarrow {}^7F_0$ line as shown in Fig. 2 in Ref. 12.

[20] B.G. Wybourne, in *Optical Properties of Ions in Crystals*, edited by H. M. Crosswhite and H. W. Moos (Interscience, New York, 1967), p. 35; B.G. Wybourne, J. Chem. Phys. **48**, 2596 (1968); Eur. J. Solid State Inorg. Chem. **28**, 19 (1991).

[21] M. C. Downer, G. W. Burdick, and D. K. Sardar, J. Chem. Phys. **89**, 1787 (1988).

[22] G. W. Burdick, M. C. Downer, and D. K. Sardar, J. Chem. Phys. **91**, 1511 (1989).

[23] V.M. Agranovich and A.A. Zakhidov, Chem. Phys. Lett. **50**, 278 (1977).

[24] P. Reineker and V.I. Yudson, Phys. Rev. B **63**, 233101 (2001).

[25] V.S. Vikhnin, G.K. Liu, and J.V. Beitz, Phys. Lett. A **287**, 419 (2001).

[26] V.S. Vikhnin, A.A. Kaplyanskii, A.B. Kutsenso, G.K. Liu, J.V. Beitz, and S.E. Kapphan, J. Lumin. **94-95**, 775 (2001).

[27] V.S. Vikhnin, R.I. Eglitis, S.E. Kapphan, and G. Borstel, and E.A. Kotomin, Phys. Rev. B **65**, 104304 (2002).

[28] S.T. Li, G.K. Liu, and W. Zhao, Opt. Lett. **24**, 838 (1999).

[29] G.K. Liu, S.T. Li, and J.V. Beitz, J. Lumin. **83-84**, 343 (1999).

[30] X.Y. Chen and G.K. Liu, J. Solid State Chem. (in press).

[31] G.K. Liu and S.T. Li (unpublished).

[32] E. Radzhabov and V. Otroshok, J. Phys. Chem. Solids **56**, 1 (1995).

[33] M. Bettinelli and C.D. Flint, J. Phys.: Condens. Matter **3**, 7053 (1991).

[34] F. Kellendonk and G. Blasse, J. Chem. Phys. **75**, 561 (1981).

[35] M. Buijs and G. Blasse, J. Lumin. **34**, 263 (1986).

[36] M. Buijs, G. Blasse, and L.H. Brixner, Phys. Rev. B **34**, 8815 (1986).

[37] M. Buijs, A. Meijerink, and G. Blasse, J. Lumin. **37**, 9 (1987).

[38] M. Inokuti and F. Hirayama, J. Chem. Phys. **43**, 1978 (1965).

[39] W.M. Yen, in *Spectroscopy of Solids Containing Rare Earth Ions*, edited by A.A. Kaplyanskii and R.M. Macfarlane (North-Holland, Amsterdam, 1987), p. 185.

[40] D.L. Huber, in *Laser Spectroscopy of Solids*, edited by W.M. Yen and P.M. Selzer (Springer, New York, 1981), p. 83.

[41] T. Holstein, S.K. Lyo, and R. Orbach, in *Laser Spectroscopy of Solids*, edited by W.M. Yen and P.M. Selzer (Springer, New York, 1981), p. 39.

[42] N.T. McDevitt and A.D. Davidson, J. Opt. Soc. Am. **56**, 636 (1966).

[43] K.R. Balasubramanian and T.M. Haridasan, J. Phys. Chem. Solids **42**, 667 (1981).

[44] M. Sauvage, Acta Crystallogr., Sect. B: Struct. Crystallogr. Cryst. Chem. **B30**, 2786 (1974).

[45] S. Schweizer, U. Rogulis, K.S. Song, and J-M Spaeth, J. Phys.: Condens. Matter **12**, 6237 (2000).

[46] T. Hoshina, S. Imanaga, and S. Yokono, J. Lumin. **15**, 455 (1977).

[47] R.P. Leavitt, J. Chem. Phys. **77**, 1661 (1982).

[48] G. Blasse, Struct. Bonding (Berlin) **26**, 43 (1976).

[49] M.Z. Su and X.P. Sun, Mater. Res. Bull. **22**, 879 (1987).

[50] W. Chen and M.Z. Su, Chinese J. Lumin. **14**, 211 (1993).

[51] C.K. Jørgensen, in *Orbitals in Atoms and Molecules* (Academic Press, New York, 1962); in *Solid State Physics*, Vol. 13, edited by F. Seitz and D. Turnbull (Academic Press, New York, 1962), p. 375.

[52] B.Z. Malkin, in *Spectroscopy of Solids Containing Rare Earth Ions*, edited by A.A. Kaplyanskii and R.M. Macfarlane (North-Holland, Amsterdam, 1987), p. 13.

[53] R.N. Bhargava, D. Gallagher, X. Hong, and A. Nurmikko, Phys. Rev. Lett. **72**, 416 (1994).

[54] A.A. Bol and A. Meijerink, Phys. Rev. B **58**, R15997 (1998).

[55] N. Murase, R. Jagannathan, Y. Kanematsu, M. Watanabe, K. Kurita, K. Hirata, T. Yazawa, and T. Kushida, J. Phys. Chem. B **103**, 754 (1999).

[56] B.A. Smith, J.Z. Zhang, A. Joly, and J. Liu, Phys. Rev. B **62**, 2021 (2001).

[57] R.N. Bhargava, J. Lumin. **70**, 85 (1996).

[58] A.A. Bol, R. van Beek, and A. Meijerink, Chem. Mater. **14**, 1121 (2002).